



1 **Formation of Chlorinated Organic Compounds from Cl Atom-Initiated**  
2 **Reactions of Aromatics and Their Detection in Suburban Shanghai**

3 **Chuang Li<sup>1</sup>, Lei Yao<sup>1,2\*</sup>, Yuwei Wang<sup>1</sup>, Mingliang Fang<sup>1</sup>, Xiaojia Chen<sup>1</sup>, Lihong Wang<sup>1</sup>,**  
4 **Yueyang Li<sup>1</sup>, Gan Yang<sup>1</sup>, Lin Wang<sup>1,2,3,4,5\*</sup>**

5 <sup>1</sup> Shanghai Key Laboratory of Atmospheric Particle Pollution and Prevention (LAP<sup>3</sup>),  
6 Department of Environmental Science and Engineering, Jiangwan Campus, Fudan  
7 University, Shanghai 200438, China

8 <sup>2</sup> Shanghai Institute of Pollution Control and Ecological Security, Shanghai 200092, China

9 <sup>3</sup> IRDR International Center of Excellence on Risk Interconnectivity and Governance on  
10 Weather/Climate Extremes Impact and Public Health, Fudan University, Shanghai 200438,  
11 China

12 <sup>4</sup> National Observations and Research Station for Wetland Ecosystems of the Yangtze Estuary,  
13 Shanghai, 200433, China

14 <sup>5</sup> Collaborative Innovation Center of Climate Change, Nanjing, 210023, China

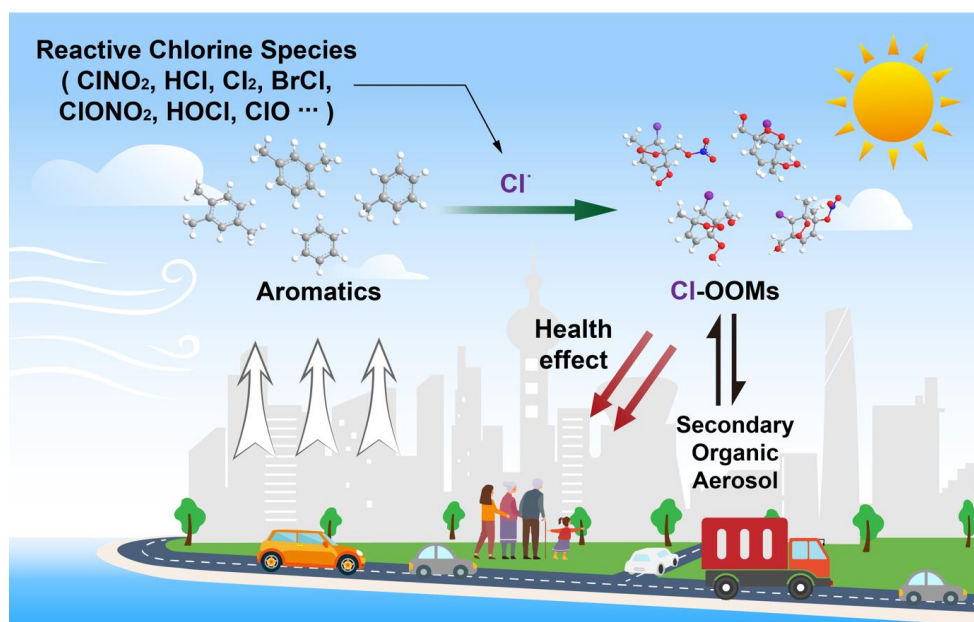
15  
16 *\*Corresponding Author: L.Y., email, lei\_yao@fudan.edu.cn; phone, +86-21-31243568*

17 *L.W., email, lin\_wang@fudan.edu.cn; phone, +86-21-31243568*

18  
19 **Abstract.** Chlorine (Cl) atoms generated from the photolysis of atmospheric reactive  
20 chlorine species can rapidly react with various volatile organic compounds (VOCs), forming  
21 chlorine- and non-chlorine-containing low-volatile oxygenated organic molecules. Yet, the  
22 formation mechanisms of chlorine-containing oxygenated organic molecules (Cl-OOMs) from  
23 reactions of Cl atoms with aromatics in the presence and absence of NO<sub>x</sub> are not fully  
24 understood. Here, we investigated Cl-OOMs formation from Cl-initiated reactions of three  
25 typical aromatics (i.e., toluene, m-xylene, and 1,2,4-trimethylbenzene (1,2,4-TMB)) in the  
26 laboratory and searched for ambient gaseous Cl-OOMs in suburban Shanghai. From our  
27 laboratory experiments, 19 Cl-containing peroxy radicals and a series of Cl-OOMs originating  
28 from the Cl-addition-initiated reaction were detected, which provides direct evidence that the  
29 Cl-addition-initiated reaction is a non-negligible pathway. In addition, a total of 51 gaseous Cl-  
30 OOMs were identified during the winter in suburban Shanghai, 38 of which were also observed  
31 in laboratory experiments, hinting that Cl-initiated oxidation of aromatics could serve as a  
32 source of Cl-OOMs in an anthropogenically influenced atmosphere. Toxicity evaluation of



33 these Cl-OOMs shows potential adverse health effects. These findings demonstrate that Cl-  
 34 OOMs can be efficiently formed via the Cl-addition pathway in the reactions between aromatics  
 35 and Cl atoms and some of these Cl-OOMs could be toxic.



36



## 37 1. INTRODUCTION

38 Atmospheric chlorine atoms (Cl), together with hydroxyl radicals (OH), ozone (O<sub>3</sub>), and nitrate  
39 radicals (NO<sub>3</sub>), play vital roles in transforming volatile organic compounds (VOCs), leading to  
40 the formation of oxygenated organic molecules (OOMs) and secondary organic aerosol  
41 (SOA)(Priestley et al., 2018; Shang et al., 2021; Tham et al., 2016; Thornton et al., 2010). The  
42 involvement of Cl atoms in atmospheric chemical processes was conventionally thought to be  
43 confined to the oceanic boundary layer (Keene et al., 1999; Knipping et al., 2000). Estimated  
44 Cl atom concentrations in the coastal region ranged from 10<sup>2</sup> to 10<sup>5</sup> molecules cm<sup>-3</sup> (Thornton  
45 et al., 2010; Wingenter et al., 2005). Recently, a number of reactive chlorine species, such as  
46 nitryl chloride (ClNO<sub>2</sub>), chlorine nitrate (ClONO<sub>2</sub>), hypochlorous (HOCl), chlorine (Cl<sub>2</sub>),  
47 bromine chloride (BrCl), and hydrochloric acid (HCl), were found to lead to high  
48 concentrations of Cl atoms in the urban and suburban atmospheres (Breton et al., 2018; Peng  
49 et al., 2020; Priestley et al., 2018). During the daytime, peak Cl atom concentrations can reach  
50 10<sup>6</sup> molecules cm<sup>-3</sup> (Wang et al., 2023). which is still less than the global average concentrations  
51 of OH radicals (Breton et al., 2018; Liu et al., 2017). Nonetheless, the reaction rate coefficients  
52 of VOCs with Cl atoms are generally 1-2 orders of magnitude larger than those of OH radicals,  
53 which can partially compensate for the lower concentration of Cl atoms when determining the  
54 relative importance of different reactive loss pathways of VOCs (Chen et al., 2023; Riva et al.,  
55 2015; Wang et al., 2005).

56 Apart from H-abstraction, Cl atoms can be added to VOCs forming chlorine-containing  
57 oxygenated organic molecules (Cl-OOMs) in reactions of VOCs with Cl atoms. For small  
58 alkenes (e.g., isoprene), the reaction mechanism is dominated by Cl-addition to the double bond,  
59 with some allylic hydrogen abstraction (approximately 15% for isoprene at 1 atm) (Finlayson-  
60 Pitts et al., 1999; Orlando et al., 2003; Ragains and Finlayson-Pitts, 1997). For larger biogenic  
61 VOCs (e.g., β-pinene), which contain a greater number of abstractable hydrogen atoms, H-  
62 abstraction becomes more significant; for instance, H-abstraction is thought to account for half  
63 of the overall initiation reactions (Finlayson-Pitts et al., 1999). Overall, both Cl-addition and  
64 H-abstraction pathways coexist for biogenic VOCs, with the Cl-addition pathway possibly



65 being the more dominant pathway, such as isoprene (Wang et al., 2022) and d-limonene (Wang  
66 et al., 2019).

67 Given the ubiquitous existence of aromatics in the urban air and the recent detection of  
68 reactive chlorine species that are precursors of Cl atoms in the same atmosphere, the reaction  
69 mechanisms of aromatics and Cl atoms should be of concern. Although the reaction rate  
70 coefficient of benzene with Cl atoms under normal atmospheric conditions is relatively slow  
71 ( $1.3 \times 10^{-15} \text{ cm}^3 \text{ molecule}^{-1} \text{ s}^{-1}$ ) and this reaction is insignificant in the ambient atmosphere, its  
72 reaction mechanism provides valuable insights into reaction pathways of Cl atoms and  
73 aromatics (Shi and Bernhard, 1997). Sokolov *et al.* proposed that  $\text{C}_6\text{H}_6\text{Cl}$  radicals, formed  
74 through a Cl-addition pathway in reactions of Cl atoms and benzene, can either decompose  
75 back to benzene or further react in a non-aromatizing manner (Sokolov et al., 1998). In contrast,  
76 toluene, xylene, and trimethylbenzene react with Cl atoms at faster rates, urging a better  
77 understanding of their reaction mechanisms. Using the density functional theory and the  
78 conventional transition state theory, Huang *et al.* investigated the Cl-toluene reaction (Huang  
79 et al., 2012). Their findings indicate that the reaction rate coefficient for the H-abstraction  
80 pathway ( $5.58 \times 10^{-11} \text{ cm}^3 \text{ molecule}^{-1} \text{ s}^{-1}$ ) is substantially higher than that for the Cl- addition  
81 pathway ( $0.91 \times 10^{-11} \text{ cm}^3 \text{ molecule}^{-1} \text{ s}^{-1}$ ), highlighting the significance of the H-abstraction  
82 pathway that accounts for approximately 86% of Cl-initiated reactions. Studies employing gas  
83 chromatography-mass spectrometry (GC-MS) to examine products of Cl-initiated reactions of  
84 toluene and iodide-based chemical ionization mass spectrometry (I-CIMS) to analyze products  
85 of Cl-initiated reactions of m-xylene, have both predominantly detected chlorine-free  
86 oxygenated organic compounds, which were supposed as main products (Cai et al., 2008; Wang  
87 et al., 2005). These results have guided atmospheric models to integrate the H-abstraction as  
88 the primary reaction pathway in their analytical frameworks (Ma et al., 2023; Peng et al., 2022).  
89 However, studies focusing on the Cl-addition pathway and its related products are sparse, and  
90 the significance of the Cl-addition pathway in the atmospheric reactions of Cl atoms and  
91 aromatics remains elusive. Over the past decade, thanks to the development of nitrate-based  
92 chemical-ionization atmospheric-pressure-interface long-time-of-flight mass spectrometers



93 (nitrate-Cl-API-LToF), there have been significant advancements in the detection of highly  
94 oxygenated organic molecules and radicals, which is crucial for elucidating the mechanisms of  
95 Cl-initiated reactions with VOCs (Bianchi et al., 2019; Ehn et al., 2010). The formation of  
96 highly oxygenated organic products, including Cl-containing ones from the reactions of  
97 biogenic VOCs with Cl atoms, were gradually revealed, whereas whether or not significant  
98 amounts of Cl-containing highly oxygenated organics and radicals can be formed from Cl atoms  
99 and aromatics remains unclear (Wang et al., 2020).

100 OOMs can lead to potential air quality, climate, and health effects. Due to their low volatility,  
101 OOMs have been identified as dominant precursors for the growth of newly formed particles  
102 and formation of SOAs, which are known for their negative effect on air quality and climate  
103 impacts (Ehn et al., 2014; Kulmala et al., 2013). Compared to non-chlorine-containing OOMs  
104 (non-Cl-OOMs), Cl-OOMs formed through the introduction of chlorine substituents make  
105 organic compounds more lipophilic, facilitating their interactions with hydrophobic sites and  
106 promoting enzymatic biotransformation in general, which can lead to adverse health effect in  
107 turn (Henschler, 1994). Therefore, field and laboratory studies for characteristics and sources  
108 of Cl-OOMs from the reactions of Cl-aromatics and their risk assessment upon human  
109 atmospheric exposure should be carried out.

110 In this study, we investigated non-Cl-OOMs and Cl-OOMs formation mechanisms from Cl-  
111 initiated reactions of toluene, m-xylene, and 1,2,4-trimethylbenzene (1,2,4-TMB) in the  
112 presence and absence of NO<sub>x</sub> in a laboratory flow reactor, using a nitrate-Cl-API-LToF  
113 (Aerodyne Research, Inc. USA, and ToFwerk AG, Switzerland) and a Vocus proton-transfer-  
114 reaction long-time-of-flight mass spectrometer (Vocus-PTR-LToF) (ToFwerk AG,  
115 Switzerland). In addition, the nitrate Cl-API-LToF was also deployed in a field campaign in  
116 suburban Shanghai during winter to search for ambient gaseous Cl-OOMs. The toxicity of  
117 selected Cl-OOMs, which were simultaneously detected both in laboratory experiments and  
118 ambient observations, was evaluated by computational toxicity.

## 119 2. MATERIALS AND METHODS

### 120 2.1. Experimental Set-up in the Laboratory.



121 A general scheme of the experimental setup is shown in Figure S1. Simulation experiments  
 122 were conducted in a 6 L quartz flow tube reactor with a total flow rate of 10 L min<sup>-1</sup>, resulting  
 123 in a residence time of ~36 seconds. This flow tube is covered by aluminum composite panels  
 124 to avoid room light. Zero air with relative humidity (RH) less than 1% generated from a Zero  
 125 Air Generator (AADC Instruments, Inc. USA) was used as carrier gas. The reaction  
 126 temperature was maintained at around 20°C.

127 Gaseous aromatics were prepared from their standards (toluene, ≥ 99.0%, Aladdin; m-xylene,  
 128 ≥ 99.0%, Aladdin; 1,2,4-TMB, ≥ 99.5%, Aladdin) together with high-purity nitrogen gases. Cl  
 129 atoms were produced by photolysis of chlorine (Cl<sub>2</sub>, Shanghai Wetry Standard Reference Gas  
 130 Analytical Technology Co., LTD) using 350 nm UV lights. In experiments with NO<sub>x</sub>, NO (Air  
 131 Liquid Co., LTD) was added into the flow tube to produce and sustain NO<sub>x</sub> mixing ratios that  
 132 were sufficiently high to be a competitive sink for RO<sub>2</sub> radicals. RH is controlled by changing  
 133 zero air flowrates through the water bubbler. Before each experiment, the wall of the flow tube  
 134 was cleaned with a water/alcohol solution and then purged with zero air for over 1 hour.

135 The concentration of Cl atoms was controlled by adjusting the flow rate of Cl<sub>2</sub>. The mean  
 136 concentrations of Cl atoms were determined according to Eq.(1) using reaction rate coefficients  
 137  $k$  of  $6.2 \times 10^{-11} \text{ cm}^3 \text{ molecule}^{-1} \text{ s}^{-1}$ ,  $1.35 \times 10^{-10} \text{ cm}^3 \text{ molecule}^{-1} \text{ s}^{-1}$ , and  $2.42 \times 10^{-10} \text{ cm}^3 \text{ molecule}^{-1}$   
 138  $\text{s}^{-1}$  for reactions between Cl atoms and toluene, m-xylene, and 1,2,4-TMB, respectively (Wang  
 139 et al., 2005), as follows:

$$140 \quad [Cl] = -1/kt \times \ln([Aromatics]_t/[Aromatics]_0) \quad \text{Eq. (1)}$$

141 where  $[Aromatics]_0$  and  $[Aromatics]_t$  are the initial concentration and the concentration  
 142 after a reaction time  $t$  of aromatic precursors, respectively.  $[Cl]$  is the estimated concentration  
 143 of Cl atoms in the flow tube. In our flow tube experiments, the extent of oxidation is quantified  
 144 using the parameter of Cl exposure, defined as  $[Cl]$  multiplied by the reaction time  $t$ . Cl  
 145 exposures in our experiments were in the range of  $(1.2\text{-}2.0) \times 10^9 \text{ molecules cm}^{-3} \text{ s}$ , equivalent  
 146 to atmospheric oxidation times of roughly 0.6-1.3 hours for aromatics at a daytime Cl atom  
 147 concentration of  $5 \times 10^5 \text{ molecules cm}^{-3}$  (Chang et al., 2004; Tham et al., 2016; Wang et al.,  
 148 2023).



149 A Vocus-PTR-LToF and a nitrate-CI-APi-LToF (more details refer to Text S1 & Figure S2  
 150 in Supplemental Information) were simultaneously deployed to detect aromatic precursors and  
 151 gaseous OOM products, respectively. Their working principles were described in details  
 152 elsewhere (Eisele and Tanner, 1993; Krechmer et al., 2018). Signals of aromatic precursors and  
 153 reaction products measured from the zero air were treated as their background. The resolving  
 154 power of the nitrate CI-APi-LToF was up to around 8000 for ions with  $m/z$  larger than 200 Th.  
 155 The ions of  $\text{NO}_3^-$ ,  $\text{HNO}_3 \cdot \text{NO}_3^-$ , and  $\text{C}_6\text{H}_5\text{NO}_3 \cdot \text{NO}_3^-$  were selected for mass calibration, and the  
 156 calibration error is less than 1 ppm. When identifying the OOM signal peaks, the error is limited  
 157 below 4 ppm.

158 OOM concentrations are estimated by Eq. (2) (Kürten et al., 2016),

$$159 \quad [\text{OOMs}] = C \times \frac{\text{OOM} \cdot \text{NO}_3^-}{\text{NO}_3^- + \text{HNO}_3 \cdot \text{NO}_3^- + (\text{HNO}_3)_2 \cdot \text{NO}_3^-} \times T \quad \text{Eq. (2)}$$

160 where  $\text{OOM} \cdot \text{NO}_3^-$ ,  $\text{NO}_3^-$ ,  $\text{HNO}_3 \cdot \text{NO}_3^-$ , and  $(\text{HNO}_3)_2 \cdot \text{NO}_3^-$  represent signals of corresponding  
 161 ions in units of counts per second (cps). OOMs with an oxygen content of equal to or more than  
 162 6 (i.e., highly oxygenated organic molecules, HOMs) are assumed to cluster with  $\text{NO}_3^-$  at the  
 163 same rate coefficient as that of sulfuric acid ( $\text{H}_2\text{SO}_4$ ), i.e., both at collision-limited rates  
 164 (Bianchi et al., 2019; Ehn et al., 2010). Therefore, the calibration factor  $C$  for sulfuric acid is  
 165 adopted as that of OOMs (Kürten et al., 2011, 2012). It should be noted we also used the same  
 166 calibration factor  $C$  for quantification of OOMs with an oxygen number of less than 6, which  
 167 may lead to relatively high uncertainties (Alage et al., 2024). A mass-dependent transmission  
 168 correction factor  $T$  of our instrument is also taken into account in this study (Heinritzi et al.,  
 169 2016). The mass-dependent transmission correction factor is instrument-specific and  
 170 determined by depleting the primary ion with a series of perfluorinated acids and comparing  
 171 the primary ion signal depletion with the product signal increase (which would match for  
 172 equivalent transmission efficiency) (Lu et al., 2020).

173 In addition, a  $\text{NO}_x$  monitor (Thermo, 49i) was utilized to measure  $\text{NO}_x$  concentrations in  
 174 laboratory experiments. A nano-SMPS (Scanning Mobility Particle Sizer with a nano  
 175 Differential Mobility Analyzer, TSI, USA) together with a PSM (Particle Size Magnifier,



176 Airmodus, Finland) were used to detect particles in the range of sub-3 nm to 60 nm, indicating  
177 the absence of newly formed particles during all experiments.  
178 Table 1 summarizes experimental conditions including mixing ratios of aromatic precursors  
179 (i.e., toluene, m-xylene, and 1,2,4-TMB), NO<sub>x</sub>, and RH.





**Table 1.** Summary of experimental conditions in the laboratory experiments.

Exp.	Precursor	Initial precursor concentration (ppb)	Initial NO <sup>a</sup> (ppb)	Estimated Cl exposure ( $\times 10^6$ molecule cm <sup>-3</sup> s)	RH <sup>b</sup> (%)	Non-Cl-OOMs molar yield (%)	Cl-OOMs molar yield (%)	Ratio (Cl-OOMs/ Total OOMs, %)	Ratio (Dimer/ Monomer, %) <sup>c</sup>
1	Toluene	80	0	2.0	<1	5.1	2.4	32	3.5
2	Toluene	80	0	1.2	60	0.7	0.3	31	2.0
3	Toluene	84	45	2.7	<1	6.8	2.6	28	1.7
4	Toluene	80	40	1.6	60	1.8	0.8	29	1.0
5	m-Xylene	87	0	2.0	<1	0.6	0.5	43	3.2
6	m-Xylene	87	0	1.6	68	0.3	0.2	44	2.6
7	m-Xylene	90	45	1.7	<1	1.4	0.6	31	0.9
8	m-Xylene	87	50	2.3	35	1.1	0.5	32	1.2
9	1, 2, 4-TMB	98	0	1.4	<1	0.5	0.3	34	2.1
10	1, 2, 4-TMB	103	0	1.4	30	0.3	0.2	35	1.4
11	1, 2, 4-TMB	93	40	2.2	<1	1.5	0.7	31	0.8
12	1, 2, 4-TMB	109	55	2.2	30	1.0	0.6	37	0.6

<sup>a</sup> In the presence of NO experiments, there is OH chemistry was involved in Cl-aromatics reactions and its influence can lead to relatively high uncertainty in the molar yields reported in the table for pathways influenced by OH chemistry. Approximately 90% of NO was converted into NO<sub>2</sub> after the UV light was turned on.

<sup>b</sup> Relative humidity.

<sup>c</sup> The molar yield ratios of total OOM dimers to monomers. Monomers are defined as molecules with a carbon number equal to the carbon number of aromatic precursor (nC), and dimers are defined as molecules with carbon numbers ranging from 2nC -1 to 2nC +1.



## 2.2. Field measurements.

A field campaign was conducted from December 14<sup>th</sup>, 2022, to February 2<sup>nd</sup>, 2023, at the Dianshan Lake (DSL) Air Quality Monitoring Supersite in suburban Shanghai, China (31.10°N, 120.98°E). This monitoring site is frequently impacted by regional transport and experiences episodes of anthropogenic pollution. A detailed description of this site can be found elsewhere (Wu et al., 2023; Yang et al., 2022, 2023). A Vocus-PTR-LToF and a nitrate-CI-API-LToF were both deployed in this field campaign to detect aromatics and Cl-OOMs, respectively. The detailed description of nitrate-CI-API-LToF and Vocus-PTR-LToF, and their calibration in the field measurement are shown in the Supplemental Information (Text S2).

## 2.3. Heath effect estimation.

A number of Cl-OOMs were assessed using the Estimation Program Interface Suite (EPI, V. 4.11) and Toxicity Estimation Software Tool (T.E.S.T., V. 5.1.2) software provided by the United States Environmental Protection Agency (EPA), to estimate their persistence, bioaccumulation, and toxicity through calculated half-life for reactions with OH, bioconcentration factors (BCF), oral rat pLD<sub>50</sub> (-log<sub>10</sub>(pred), mol/kg), developmental toxicity, and mutagenicity. The models utilized the SMILES (Simplified Molecular Input Line Entry System) notation of the target compounds as input for the prediction.

# 3. RESULTS AND DISCUSSION

## 3.1. OOM molar yields.

The molar yields of OOMs are determined as OOMs formed ( $\Delta M$ , molar cm<sup>-3</sup>) divided by precursor reacted ( $\Delta Ar$ , molar cm<sup>-3</sup>):

$$\text{Molar yield} = \frac{\Delta M}{\Delta Ar} \quad \text{Eq. (3)}$$

Table 1 summarizes non-Cl-OOMs' and Cl-OOMs' molar yields and OOMs' dimer-to-monomer ratios from our laboratory experiments. The molar yields of non-Cl-OOMs and Cl-OOMs from reactions of three aromatic precursors with Cl atoms in the absence of NO<sub>x</sub> are within the ranges of 0.3-5.1% and 0.2-2.4%, respectively. These values are comparable with previously reported: HOM molar yields (0.8-4.0%) detected by nitrate-CI-API-LToF for the reactions between  $\alpha$ -



pinene and Cl atoms (Wang et al., 2020) and non-Cl-OOMs molar yields (4.4-8.8%) detected by  $\text{H}_3\text{O}^+$ -Chemical Ionization Mass Spectrometry ( $\text{H}_3\text{O}^+$ -CIMS) for the reactions between m-xylene and Cl atoms (Bhattacharyya et al., 2023). The low molar yields observed in both this study and previous studies may be attributed to the preference of different detection techniques. Nevertheless, the observed ratio of Cl-OOMs to non-Cl-OOMs, ranging from 29% to 44% (Table 1), further indicates the non-negligibility of the Cl-OOMs products among the total OOMs products. In the presence of 40-55 ppb  $\text{NO}_x$ , our flow tube experiments show that the molar yields of non-Cl-OOMs and Cl-OOMs from three aromatics are within the ranges of 1.0-6.8% and 0.5-2.6%, respectively. The addition of  $\text{NO}_x$  can slightly increase the molar yields of both non-Cl-OOMs and Cl-OOMs.

Typically, the fate of peroxy radicals in flow tube experiments is largely influenced by their reactions with other  $\text{RO}_2$ ,  $\text{HO}_2$ , or  $\text{NO}$  species, which are contingent upon the specific experimental conditions (Bianchi et al., 2019; DeMore et al., 1997). In experiments without  $\text{NO}_x$ , while the termination of  $\text{RO}_2$  was primarily anticipated to be governed by  $\text{RO}_2$ - $\text{RO}_2$  and  $\text{HO}_2$ - $\text{RO}_2$  reactions. However, after the addition of  $\text{NO}_x$ , the reaction between  $\text{RO}_2$  and  $\text{NO}$  tended to predominate, leading to a reduction in the dimer-to-monomer ratio by 50.5% (Exp. 3 and Exp. 1 in Table 1).

In contrast to OH reaction, the presence of Cl, ClO, and  $\text{Cl}_2$  in chlorine-involved reaction may introduce additional reaction pathways related to Cl-OOM formation. However, these pathways make only minor contributions to the formation of Cl-OOMs under our experimental conditions (see Text S4 in Supplemental Information for detailed analysis).

Although both the non-Cl-OOMs and Cl-OOMs molar yields increased in the presence of  $\text{NO}_x$ , the ratio of Cl-OOMs to the total OOMs decreased when  $\text{NO}_x$  was added. This phenomenon can be ascribed to the critical involvement of OH chemistry, stemming from the  $\text{NO}+\text{HO}_2$  reaction. The additional OH radicals can contribute to the formation of non-Cl-OOMs, as supported by recent experimental and modeling studies on the reaction dynamics between Cl atoms and isoprene (Wang et al., 2022). For our experiments, as  $\text{NO}_x$  was added into the flow tube, the concurrent presence of Cl atoms, OH radicals, and aromatics led to a notable

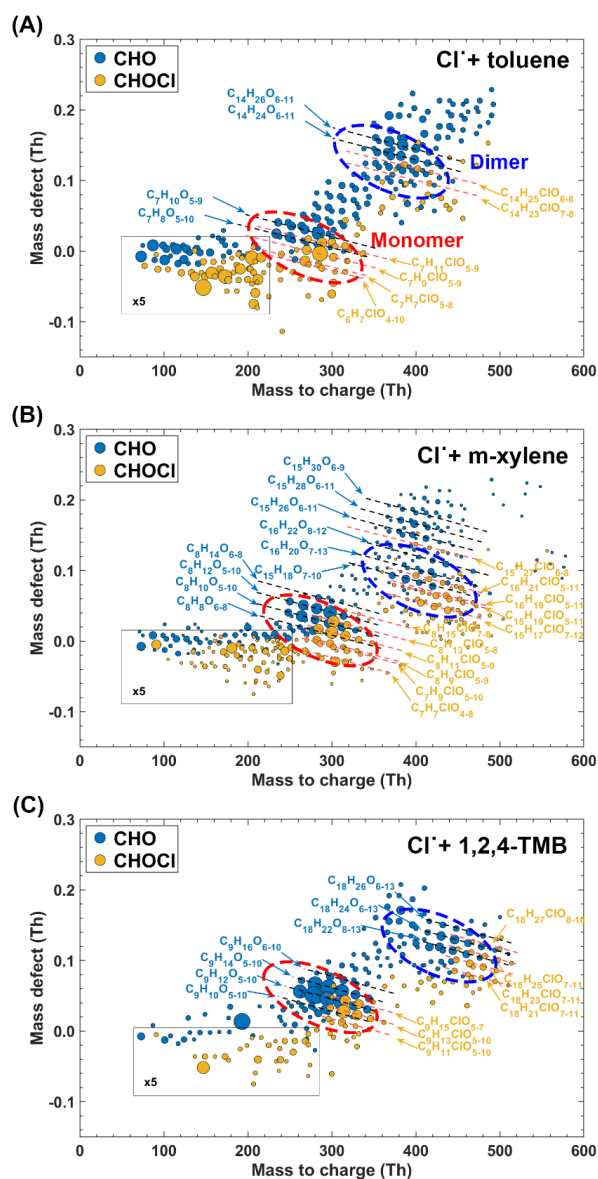


241 increase in the total OOM molar yields, ranging from 25 to 187%, while reducing the ratios of  
 242 Cl-OOMs to the total OOMs by approximately 9-28% (Table 1). It should be noted that molar  
 243 yields reported in Table 1 with high uncertainty due to OH chemistry in the presence of NO<sub>x</sub>.  
 244 Besides, high RH leads to low molar yields, which may be attributed to the depressed detection  
 245 efficiency of OOMs and the elevated vapor wall loss under humid conditions (Huang et al.,  
 246 2018). The product distribution remains unchanged under high humidity conditions (see Figure  
 247 1B and Figure S3), indicating that the presence of water does not significantly influence the  
 248 reaction between Cl atoms and aromatics.

### 249 **3.2. Characteristics of OOM products and peroxy radicals.**

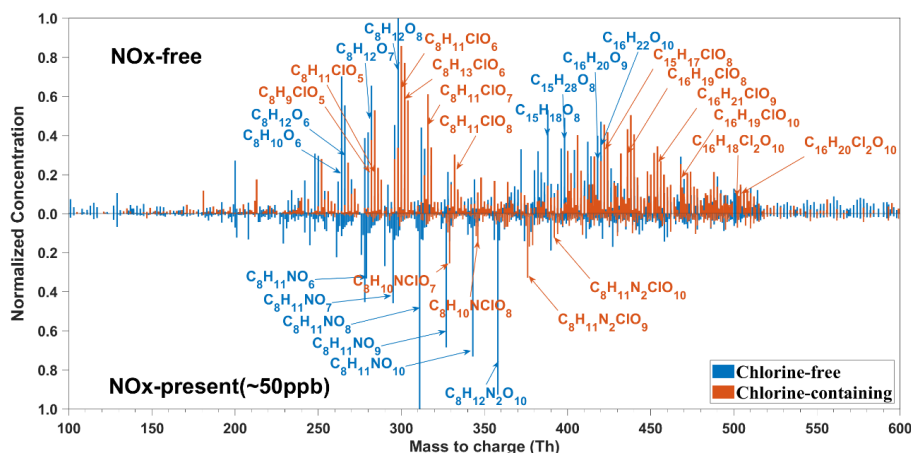
250 Mass defect plots of stabilized products from reactions between toluene (Exp.1 in Table1),  
 251 m-xylene (Exp.5 in Table1), and 1,2,4-TMB (Exp.9 in Table1) and Cl atoms in the absence of  
 252 NO<sub>x</sub> are shown in Figure 1. These products display similar distribution patterns, consisting of  
 253 monomers (with carbon numbers equal to carbon numbers of the precursor, nC) and dimer  
 254 products (with carbon numbers ranging from 2nC -1 to 2nC +1). The ratio of dimer products to  
 255 monomer products are 3.5%, 3.2%, and 2.1% for reactions of toluene, m-xylene, and 1,2,4-  
 256 TMB with Cl atoms, respectively. Meanwhile, the products also can be classified into two  
 257 groups: non-Cl-OOMs in blue and Cl-OOMs in orange in Figure 1. In general, the total  
 258 concentration of Cl-OOMs is lower than that of non-Cl-OOMs. Specifically, the concentrations  
 259 of Cl-OOMs account for 47%, 91%, and 52% of the non-Cl-OOMs in the toluene, p-xylene,  
 260 and 1,2,4-trimethylbenzene experiments, respectively. Both non-Cl-OOMs and Cl-OOMs  
 261 products can be categorized into several bands, as indicated by the dashed lines in Figure 1,  
 262 each of which comprises compounds with varying numbers of oxygen atoms.

263



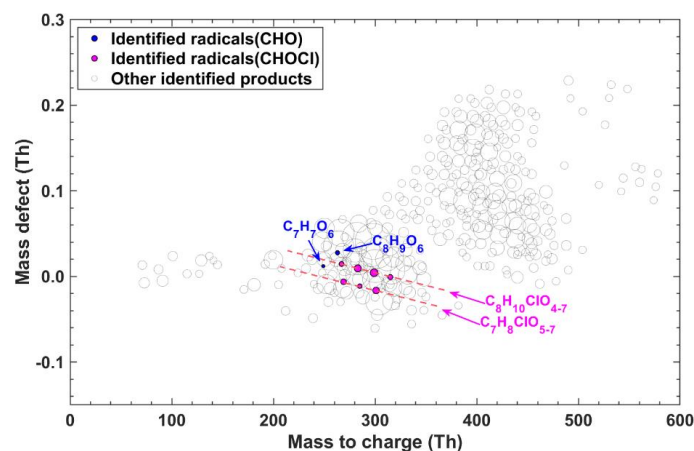


270 The mass spectrum of the detected OOMs monomer and dimer products from the reaction  
 271 between m-xylene and Cl atoms with and without NO<sub>x</sub> (Exp. 5&7 in Table 1) are shown in  
 272 Figure 2. Without NO<sub>x</sub>, dominant monomer products for non-Cl-OOMs included C<sub>8</sub>H<sub>10</sub>O<sub>6</sub> and  
 273 C<sub>8</sub>H<sub>12</sub>O<sub>6-8</sub>, whereas for Cl-OOMs, C<sub>8</sub>H<sub>11</sub>ClO<sub>6-8</sub> and C<sub>8</sub>H<sub>13</sub>ClO<sub>6-7</sub> dominated. The most  
 274 abundant dimer compounds for non-Cl-OOMs were C<sub>16</sub>H<sub>20</sub>O<sub>9</sub>, C<sub>16</sub>H<sub>22</sub>O<sub>10</sub>, and C<sub>15</sub>H<sub>18</sub>O<sub>8</sub>,  
 275 whereas for Cl-OOMs, C<sub>16</sub>H<sub>19</sub>ClO<sub>8,10</sub>, C<sub>16</sub>H<sub>21</sub>ClO<sub>9</sub>, and C<sub>15</sub>H<sub>17</sub>ClO<sub>8</sub> prevailed. Dimer products  
 276 containing two Cl atoms were also observed, exemplified by C<sub>16</sub>H<sub>18,20</sub>Cl<sub>2</sub>O<sub>10</sub>. Under NO<sub>x</sub>-  
 277 present conditions, the main non-Cl-OOMs included C<sub>8</sub>H<sub>11</sub>NO<sub>6-10</sub> and C<sub>8</sub>H<sub>12</sub>N<sub>2</sub>O<sub>10</sub>, whereas  
 278 Cl-OOMs were represented by C<sub>8</sub>H<sub>10</sub>ClNO<sub>7-8</sub> and C<sub>8</sub>H<sub>11</sub>ClN<sub>2</sub>O<sub>9-10</sub>.



280 **Figure 2.** Mass spectra of OOM products detected by a nitrate-Cl-API-LToF from the reaction of m-xylene and  
 281 Cl atoms under NO<sub>x</sub>-free and NO<sub>x</sub>-present conditions. The y-axes in both figures are standardized by setting their  
 282 maximum concentrations to 1.  
 283

284 Moreover, 26 peroxy radicals in total were observed in our flow tube experiments with three  
 285 precursors, as listed in Table S1 and illustrated in Figures 3 & S4. It is crucial to note, however,  
 286 that not every intermediate radical formed could be conclusively identified. This is primarily  
 287 due to the inherent instability and the extremely brief life span of peroxy radicals, which pose  
 288 significant challenges for their detection.



289

290 **Figure 3.** Mass defect plot of peroxy radicals detected by a nitrate-Cl-API-LToF from Cl-initiated reactions of  
 291 m-xylene without NO<sub>x</sub>. The detected products are marked by their exact mass (with NO<sub>3</sub><sup>-</sup> reagent ions) and mass  
 292 defect (exact mass subtracted by its unit mass). The lines annotate the general chemical formulas. Chlorine-  
 293 containing and non-chlorine-containing formulas are shown in different colors. The size of the circle is  
 294 proportional to the concentrations of peroxy radicals.

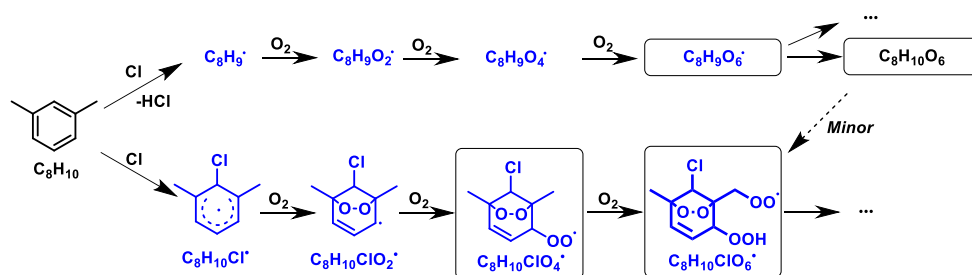
295 Take the reaction between Cl atoms and m-xylene in the absence of NO<sub>x</sub> for example, we  
 296 detected peroxy radicals including C<sub>8</sub>H<sub>10</sub>ClO<sub>4-7</sub>, C<sub>7</sub>H<sub>8</sub>ClO<sub>5-7</sub>, C<sub>8</sub>H<sub>9</sub>O<sub>6</sub>, and C<sub>7</sub>H<sub>7</sub>O<sub>6</sub> (Figure 3).  
 297 High-resolution peak fittings of partial peroxy radicals from the raw mass spectrum obtained  
 298 by nitrate-Cl-API-LToF are shown in Figure S5. Notably, the dominant species among these  
 299 radicals was C<sub>8</sub>H<sub>10</sub>ClO<sub>6</sub>, constituting 27.4% of the total signal of identified peroxy radicals in  
 300 the reaction of Cl atoms and m-xylene and nearly three times of the C<sub>8</sub>H<sub>9</sub>O<sub>6</sub> radical signal. Also,  
 301 similar ratio rules of chlorine-containing radicals (analogy of C<sub>8</sub>H<sub>10</sub>ClO<sub>6</sub>) to non-chlorine-  
 302 containing radicals (analogy of C<sub>8</sub>H<sub>9</sub>O<sub>6</sub>) were observed for toluene (~4.2 times) and 1,2,4-TMB  
 303 (~3.8 times). Although C<sub>7</sub>H<sub>8</sub>ClO<sub>5-7</sub> radicals were also discernible, their signal intensity was  
 304 merely 22.3% of the total signal of identified peroxy radicals in the reaction of Cl atoms and  
 305 m-xylene. Non-Cl-containing radicals were also detected, albeit with substantially lower signal  
 306 values, accounting for only 15.5% of the total identified radical signals.

### 307 3.3. Formation mechanisms of Cl-OOMs

#### 308 3.3.1. Cl-addition pathway



309 Given the similar product patterns for the three precursors (toluene, m-xylene, and 1,2,4-  
 310 TMB), it is reasonable to infer that the reaction mechanisms between different aromatics and  
 311 Cl atoms are analogous. A generalized mechanism is thus proposed, elucidating the Cl-initiated  
 312 reactions of m-xylene in the absence of NO<sub>x</sub>, as depicted in Scheme 1. This scheme serves as  
 313 a representative example highlighting the potential pathways involved in the Cl-initiated  
 314 reactions of aromatics.



315

316 **Scheme 1.** Proposed reaction mechanisms of m-xylene with Cl atoms leading to the formation of OOMs. Blue  
 317 and black formulae denote radicals, and stable products, respectively. Radicals and stable products detected by  
 318 nitrate-Cl-API-LToF are marked with black boxes.

319 Although the theoretical studies by Huang *et al.* (2012) show that the Cl-addition pathway  
 320 accounts for only 14% of Cl-initiated reactions of toluene (298K), which is significantly lower  
 321 than the 86% attributed to the H-abstraction pathway, the proportion of Cl-OOMs products  
 322 from Cl-addition reaction should not be overlooked, as evidenced by the observation of peroxy  
 323 radicals and product distribution characteristics in this study (Huang *et al.*, 2012). The initial  
 324 reaction of m-xylene (C<sub>8</sub>H<sub>10</sub>) with Cl atoms can occur through two pathways: the addition  
 325 pathway, Cl-addition leading to the formation of a C<sub>8</sub>H<sub>10</sub>Cl radical (C<sub>8</sub>H<sub>10</sub>Cl·) or the H-  
 326 abstraction pathway, forming a C<sub>8</sub>H<sub>9</sub> radical (C<sub>8</sub>H<sub>9</sub>·) (Scheme 1). Then, both C<sub>8</sub>H<sub>9</sub>· and  
 327 C<sub>8</sub>H<sub>10</sub>Cl· can in turn undergo autoxidation via the formal addition of O<sub>2</sub> to produce peroxy  
 328 radicals of C<sub>8</sub>H<sub>9</sub>O<sub>6</sub>· or C<sub>8</sub>H<sub>10</sub>ClO<sub>6</sub>·. The peroxy radical C<sub>8</sub>H<sub>10</sub>ClO<sub>6</sub>· was identified as the  
 329 predominant species in terms of signal (Table S1). The signal intensity ratio of C<sub>8</sub>H<sub>10</sub>ClO<sub>6</sub>· to  
 330 C<sub>8</sub>H<sub>9</sub>O<sub>6</sub>· was around 3 in our reaction, which suggests that Cl-addition pathway could be at  
 331 least a non-negligible pathway in the initial reaction steps of Cl atoms and m-xylene, compared





332 with H-abstraction pathway. Furthermore, the signal intensity ratios of Cl-addition pathway  
333 radicals ( $C_7H_8ClO_6\cdot$  from toluene and  $C_9H_{12}ClO_4\cdot$  from 1,2,4-TMB) and H-abstraction pathway  
334 radicals ( $C_7H_7O_6\cdot$  from toluene and  $C_9H_{11}O_4\cdot$  from 1,2,4-TMB) were 4.2 and 5.6 (Table S1),  
335 respectively. Although these Cl-OOMs-to-non-Cl-OOMs signal ratios may not accurately  
336 represent their relative concentrations due to sensitivity differences of these radicals towards  
337 the reagent ions ( $(HNO_3)_{0-1}\cdot NO_3^-$ ), it is still noteworthy that these Cl-RO<sub>2</sub> overlooked in  
338 previous studies were directly observed in such a reaction system, thereby suggesting that Cl-  
339 addition pathway is indeed present in the initial reaction steps of reactions between Cl atoms  
340 and aromatics.

341 In the reaction of Cl atoms and m-xylene, a certain fraction of the peroxy radicals  
342 ( $C_8H_{10}ClO_6\cdot$ ) might also be derived from the secondary Cl-addition reaction between Cl atoms  
343 and a first-generation stabilized product  $C_8H_{10}O_6$  (Scheme 1). Indeed, it is challenging to  
344 evaluate the exact contribution from secondary Cl-addition reaction to the formation of  
345  $C_8H_{10}ClO_6\cdot$ . However, it may be indirectly assessed via the potential secondary reactions  
346 between more dominant first-generation stabilized products ( $C_8H_{12}O_x$ ) and Cl (Table S2), since  
347  $C_8H_{10}O_6$  and  $C_8H_{12}O_x$  likely react with Cl at similar rates. If secondary Cl-addition reactions  
348 were significant in the reaction system of Cl atoms and m-xylene,  $C_8H_{12}O_x$  should undergo  
349 secondary Cl-addition reactions to generate  $C_8H_{12}ClO_x$  radicals. Yet,  $C_8H_{12}ClO_x$  radicals were  
350 not detectable, which hints that secondary Cl-addition reactions could only play a minor role in  
351 our experiments. Therefore, it appears that the secondary Cl-addition reactions between  
352 stabilized products and Cl atoms are less significant compared with Cl-addition in the initial  
353 reaction steps.

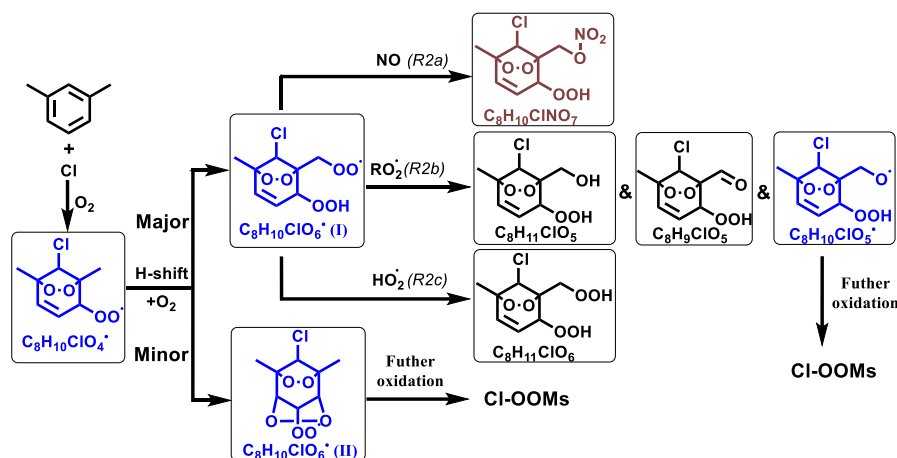
354 Recently, Jahn et al. (2024) investigated the formation of secondary organic aerosols from  
355 the reaction of ethylbenzene and Cl atoms, and attributed the observed Cl-addition products to  
356 reactions involving non-aromatic C=C bonds (Jahn et al., 2024). They claimed that OH radical  
357 existed in their experiments, due to the presence of NO<sub>x</sub>. As a result, approximately 40% of  
358 ethylbenzene reacted with Cl atoms, 30% with OH, and 30% remained unreacted. Thus, a  
359 secondary Cl addition to  $C_8H_{11}NO_6$  for reaction of ethylbenzene and Cl atoms, forming



360  $C_8H_{12}ClNO_8$ , is possible (Scheme S1). However, OH radical was expected to be minor at least  
 361 in our NO<sub>x</sub>-free experiments. Thus  $C_8H_{11}NO_6$ , as an OH addition product (Scheme S2), was  
 362 insignificant in our NO<sub>x</sub>-free reaction of m-xylene and Cl atoms (refer to Figure 2), leading to  
 363 a minor role of a secondary Cl addition to form  $C_8H_{12}ClNO_8$ . In our experiments with NO<sub>x</sub>, the  
 364 primary Cl-contain products, i.e.,  $C_8H_{10}ClNO_7$  (Scheme S3), contain two less hydrogen atoms  
 365 than  $C_8H_{12}ClNO_8$ , likely explained by the existence of one more double bond in the structure  
 366 of  $C_8H_{10}ClNO_7$ . The presence of this additional double bond excludes the possibility of a  
 367 sequential OH addition and Cl addition.

### 368 3.3.2. Autoxidation and subsequent reactions of Cl-RO<sub>2</sub>

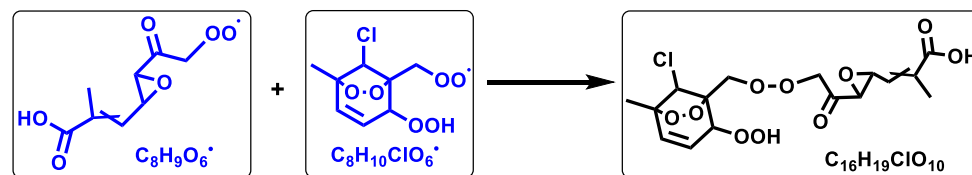
369 Scheme 2 shows a proposed reaction mechanism for the autoxidation of the main Cl-RO<sub>2</sub>  
 370 radical ( $C_8H_{10}ClO_4\cdot$ ) generated from Cl atoms and m-xylene. Autooxidation of  $C_8H_{10}ClO_4\cdot$   
 371 leads to  $C_8H_{10}ClO_6\cdot$ . There are two distinct isomeric forms of  $C_8H_{10}ClO_6\cdot$ , denoted as  
 372  $C_8H_{10}ClO_6\cdot$  (I) and  $C_8H_{10}ClO_6\cdot$  (II), which is similar to results for aromatics + OH by Molteni  
 373 et al (Molteni et al., 2018). Notably, the formation of  $C_8H_{10}ClO_6\cdot$  (II) requires a second step of  
 374 endo-cyclization, which is not competitive on account of its slow reaction rate, as inferred from  
 375 several previous studies using both experimental and theoretical approaches of OH-initiated  
 376 oxidation of aromatics (Wang et al., 2017; Xu et al., 2020). Therefore, the abundance of  
 377  $C_8H_{10}ClO_6\cdot$  (I) would likely be much higher than  $C_8H_{10}ClO_6\cdot$  (II), and our following discussion  
 378 primarily focuses on the subsequent reaction processes involving  $C_8H_{10}ClO_6\cdot$  (I). Briefly,  
 379  $C_8H_{10}ClO_6\cdot$  reacts with RO<sub>2</sub> $\cdot$  to generate  $C_8H_{9,11}ClO_5$  and  $C_8H_{10}ClO_5\cdot$  (Reaction pathway R2b)  
 380 and with an HO<sub>2</sub> radical to produce  $C_8H_{11}ClO_6$  (Reaction pathway R2c). Meanwhile,  
 381  $C_8H_{10}ClO_6\cdot$  has no more H atoms for another H-shift at an appreciable rate based on our current  
 382 understanding.(Wang et al., 2024) In the presence of NO<sub>x</sub>,  $C_8H_{10}ClO_6\cdot$  is terminated (Reaction  
 383 pathway R2a), leading to the formation of  $C_8H_{10}ClNO_7$  products.



**Scheme 2.** Reaction pathways of the bicyclic peroxy radical  $C_8H_{10}ClO_4$  in the Cl-initiated reaction of m-xylene. Blue, brown, and black formulae denote radicals, nitrogen-containing products, and Cl-OOMs products, respectively. Radicals and stable products detected by nitrate-Cl-API-LToF are marked with black boxes.

### 3.3.3. Dimer formation

The accretion reaction ( $RO_2 + R'O_2 \rightarrow ROOR' + O_2$ ) represents a pivotal source for dimer compounds, originating from highly oxidized and functionalized  $RO_2$  radicals (Ehn et al., 2014; Zhao et al., 2018). As shown in Figure 2,  $C_{16}H_{19}ClO_8$  and  $C_{16}H_{19}ClO_{10}$  are two typical accretion reaction products from reactions between Cl atoms and m-xylene without  $NO_x$ . In detail,  $C_{16}H_{19}ClO_{10}$  can be formed through the accretion reaction between  $C_8H_{10}ClO_6$  and  $C_8H_9O_6$  (Scheme 3). The formation pathways for  $C_{16}H_{19}ClO_8$  are more varied compared to that of  $C_{16}H_{19}ClO_{10}$ . It can be produced either via the accretion of a  $C_8H_{10}ClO_6$  radical with a  $C_8H_9O_4$  radical or through the reaction of a  $C_8H_{10}ClO_4$  radical with a  $C_8H_9O_6$  radical. Meanwhile,  $C_{16}H_{20}Cl_2O_{10}$ , which is also detected during the reaction, can be formed via the accretion reaction of two  $C_8H_{10}ClO_6$  radicals.



**Scheme 3.** Accretion reaction pathways of peroxy radical  $C_8H_{10}ClO_6$  and  $C_8H_9O_6$  in the Cl-initiated reaction of



401 m-xylene. Blue and black formulae denote radicals and stable products, respectively. Radicals and stable products  
 402 detected by nitrate-Cl-API-LToF are marked with black boxes.

403 Previous studies have reported dimer formation rates during the OH-initiated oxidation of  
 404 1,3,5-trimethylbenzene, ranging from  $1.4 \times 10^{-10}$  to  $25 \times 10^{-10} \text{ cm}^3 \text{ molecule}^{-1} \text{ s}^{-1}$  (Berndt et al.,  
 405 2017). Compared to the OH reaction, Cl-RO<sub>2</sub> is produced in the Cl atom reaction, but its  
 406 reaction rate in the accretion reaction remains unknown. If Cl-RO<sub>2</sub> have lower reactivity (i.e.,  
 407 slower rate coefficients) for accretion reactions compared to non-Cl-containing RO<sub>2</sub>, the same  
 408 generation rate of Cl-RO<sub>2</sub> and RO<sub>2</sub> would result in higher concentration of Cl-RO<sub>2</sub>, resulting in  
 409 the high Cl-RO<sub>2</sub> signal detected. However, the generation rate of both Cl-RO<sub>2</sub> and RO<sub>2</sub> are  
 410 currently uncertain, further complicating the determination of the chemical mechanisms of Cl-  
 411 initiated reactions even more challenging.

#### 412 **3.4. Cl-OOMs detection in suburban Shanghai.**

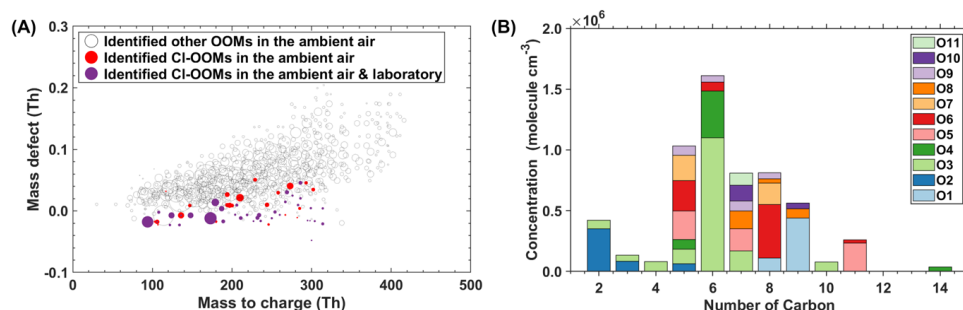
413 As shown in Figure 4A and Table S3, a total of 51 gaseous Cl-OOMs were identified during  
 414 winter in suburban Shanghai, whose high-resolution peak fittings measured by nitrate Cl-API-  
 415 LToF are shown in Figure S6. Figure S7 further demonstrates the accuracy of our peak  
 416 identification by showing the ratio of the fitted peak intensities versus the peak separation for  
 417 identified Cl-OOM peaks and adjacent ions from our ambient nitrate-Cl-API-LToF  
 418 measurements (Cubison and Jimenez, 2015). The peak separation, normalized to the half-width  
 419 at half-maximum ( $\chi = \Delta t/\text{HWHM}$ ), is greater than 1 for all Cl-OOMs. Notably, 22% of the  
 420 peaks exhibit  $\chi$  values between 1 and 2, indicating they are separable but closely spaced, while  
 421 78% of the Cl-OOMs ( $\chi > 2$ ) are well-separated peaks.

422 Ambient Cl-OOMs consist of compounds mostly with a single Cl atom and only two with  
 423 two Cl atoms. The carbon and oxygen numbers of these Cl-OOMs ranged from 2 to 14 and 1  
 424 to 11, respectively. Figure 4B shows the abundance distribution of gaseous Cl-OOMs on the  
 425 basis of carbon and oxygen numbers in their molecular formulae. Approximately 80%  
 426 concentration of the identified Cl-containing molecules is C5-C9 Cl-OOMs, among which C6-  
 427 C9 Cl-OOMs represent a large fraction of ~79 %.



428 38 Cl-OOMs observed in field measurements were also identified in our laboratory  
 429 experiments, corresponding to reaction products of Cl atoms with toluene, m-xylene, or 1,2,4-  
 430 TMB. These results indicate that ambient C6-C9 Cl-OOMs exemplified by  $C_7H_7N_2ClO_9$ ,  
 431  $C_8H_{10}NClO_7$ , and  $C_9H_{15}ClO_8$  are likely formed from Cl-initiated reactions with aromatic  
 432 compounds. On the other hand, isoprene was considered as a precursor of C5 Cl-OOMs (Breton  
 433 et al., 2018; Priestley et al., 2018; Wang and Ruiz, 2017).

434 Figure S8 shows the averaged diurnal variation of  $C_7H_7N_2ClO_9$ ,  $C_8H_{10}NClO_7$ , and  
 435  $C_9H_{15}ClO_8$  during our field campaign with rainy days excluded. Similar to previous reports in  
 436 northern Europe and Beijing (Breton et al., 2018; Priestley et al., 2018), Cl-OOMs increased  
 437 with elevated solar radiation and their peaks appeared at around 12:00 p.m. (local time) hinting  
 438 that the formation of Cl-OOMs is connected with photochemistry. This suggests that while  
 439  $ClNO_2$  photolysis is a significant early morning source of Cl atoms, other sources such as the  
 440 photolysis of  $Cl_2$ ,  $ClONO_2$ ,  $HCl$ ,  $ICl$ , and  $BrCl$  with sunlight can contribute to Cl atom  
 441 concentrations later in the day. (Peng et al., 2020)



442 **Figure 4.** (A). Mass defect plot of detected OOMs by a nitrate-Cl-API-LToF in ambient air in suburban Shanghai.  
 443 Cl-OOMs only observed in the ambient atmosphere were marked in red, and Cl-OOMs observed in both ambient  
 444 and lab were marked in purple. The size of the circle is proportional to the concentration of compounds in the  
 445 ambient. (B). Distribution of carbon and oxygen number of gas-phase Cl-OOMs identified in suburban Shanghai.  
 446 The color codes correspond to the number of oxygen atoms.

### 448 3.5. Health effect of ambient Cl-OOMs.

449 Table S5 presents a detailed toxicity estimation of various Cl-OOMs, including  $C_7H_7N_2ClO_9$ ,  
 450  $C_8H_{10}NClO_7$ , and  $C_9H_{15}ClO_8$ , which were identified in the suburban Shanghai atmosphere and  
 451 laboratory experiments. These estimations are based on the potential chemical structures of



452 these Cl-OOMs. We characterized the toxicity of these Cl-OOMs using persistence,  
453 bioaccumulative and toxic (PBT) criteria, as outlined in Table S5. Additionally, we conducted  
454 a comparative analysis of their toxicity relative to that of naphthalene, a compound whose  
455 atmospheric toxicity has been extensively studied.

456 Compounds with short OH radical reaction half-lives and bioconcentration factors (BCF) are  
457 unlikely to be persistent and bioaccumulative. Among these Cl-OOMs,  $C_8H_{10}NClO_7$  (II)  
458 exhibits the slowest degradation rate with OH radicals with a half-life of 5 days, which suggests  
459 that it is a potential new persistent pollutant (half-life > 2 days) in the atmosphere (Europe,  
460 2023).

461 As indicated by the  $pLD_{50}$  values, toxicity levels of most Cl-OOMs are lower than that of  
462 naphthalene, except for  $C_8H_{10}NClO_8$ ,  $C_8H_{10}NClO_7$  (I), and  $C_7H_7N_2ClO_8$  (Table S5). Among  
463 these compounds,  $C_8H_{10}NClO_7$  (I) is identified with the highest predicted toxicity, followed by  
464 compound  $C_8H_{10}NClO_8$ . The  $pLD_{50}$  of these compounds is categorized within level 3,  
465 signifying their potential for a considerable acute toxicity.

466 Notably, the  $pLD_{50}$  values of Cl-OOMs are found to be akin to those of naphthalene.  
467 However, given that their concentration in suburban Shanghai (0.55 ppt) is merely one percent  
468 of that of naphthalene (50 ppt) as measured in this study, the total probabilistic hazard quotient  
469 (PrHQ, defined as the product of estimated human exposure (ambient concentration) and  $pLD_{50}$   
470 in this study) of Cl-OOMs is lower. Despite this lower PrHQ, it is important to recognize that  
471 each of the evaluated Cl-OOMs may pose risks of developmental toxicity and mutagenicity,  
472 which underscores the need for a thorough understanding of the toxicological implications of  
473 Cl-OOMs in the atmosphere.

474 In summary, this study highlights the Cl-addition-initiated reaction as a non-negligible  
475 pathway in the reaction of Cl atoms with aromatics. Field measurements in suburban Shanghai  
476 revealed 51 gaseous Cl-OOM species, with 38 of these Cl-OOMs also detected in our laboratory  
477 experiments. This suggests that these Cl-OOMs likely derive from reactions between Cl atoms  
478 and aromatics. Considering the significant role of Cl atoms in daily atmospheric oxidation



479 processes, overlooking the Cl-addition pathway could lead to ignoring the formation of Cl-  
480 OOMs from aromatic compounds in the atmosphere. This study, therefore, highlights the  
481 necessity of incorporating both pathways in the models for a more accurate assessment of the  
482 atmospheric fate of Cl atoms and aromatics in urban settings. In addition, health effect  
483 evaluation indicates that all assessed Cl-OOMs may possess developmental toxicity, and nearly  
484 half of the compounds may exhibit carcinogenic effects. Considering the critical role of  
485 aromatics in the urban air and recent observations reporting increased levels of reactive chlorine  
486 species in polluted atmospheres, our study offers timely insights into the chemical processes  
487 between Cl atoms and aromatics occurring in anthropogenically influenced atmospheres and  
488 the adverse health effects of these Cl-containing reaction products.

489 **Data availability.**

490 The data used in this study are available upon request from Lei Yao (lei\_yao@fudan.edu.cn)  
491 and Lin Wang (lin\_wang@fudan.edu.cn).

492 **Author contributions.**

493 LY and LW conceived and designed this study and revised the manuscript. CL analyzed and  
494 interpreted data, drafted and revised the manuscript. CL and YW contributed to the modeling  
495 of the data. MF and XC contributed to the health effect analysis.

496 **Competing interests.**

497 The contact author has declared that none of the authors has any competing interests.

498 **Financial support.** This research was supported by the National Key Research and  
499 Development Program of China (2022YFC3704100) and the National Natural Science  
500 Foundation of China (21925601, 22376031, 92143301).

501



## 502 References

- 503 Alage, S., Michoud, V., Harb, S., Picquet-Varrault, B., Cirtog, M., Kumar, A., Rissanen, M.,  
504 and Cantrell, C.: A nitrate ion chemical-ionization atmospheric-pressure-interface time-of-  
505 flight mass spectrometer (NO<sub>3</sub>- ToFCIMS) sensitivity study, *Atmos. Meas. Tech.*, 17, 4709–  
506 4724, <https://doi.org/10.5194/amt-17-4709-2024>, 2024.
- 507 Berndt, T., Scholz, W., Mentler, B., Fischer, L., Herrmann, H., Kulmala, M., and Hansel, A.:  
508 Accretion Product Formation from Self- and Cross-Reactions of RO<sub>2</sub> Radicals in the  
509 Atmosphere., *Angewandte Chemie Int Ed Engl*, 57, 3820–3824,  
510 <https://doi.org/10.1002/anie.201710989>, 2017.
- 511 Bhattacharyya, N., Modi, M., Jahn, L. G., and Ruiz, L. H.: Different chlorine and hydroxyl  
512 radical environments impact m -xylene oxidation products, *Environ. Sci.: Atmos.*,  
513 <https://doi.org/10.1039/d3ea00024a>, 2023.
- 514 Bianchi, F., Kurtén, T., Riva, M., Mohr, C., Rissanen, M. P., Roldin, P., Berndt, T., Crounse,  
515 J. D., Wennberg, P. O., Mentel, T. F., Wildt, J., Junninen, H., Jokinen, T., Kulmala, M.,  
516 Worsnop, D. R., Thornton, J. A., Donahue, N., Kjaergaard, H. G., and Ehn, M.: Highly  
517 Oxygenated Organic Molecules (HOM) from Gas-Phase Autoxidation Involving Peroxy  
518 Radicals: A Key Contributor to Atmospheric Aerosol, *Chem Rev*, 119, 3472–3509,  
519 <https://doi.org/10.1021/acs.chemrev.8b00395>, 2019.
- 520 Breton, M. L., Hallquist, Å. M., Pathak, R. K., Simpson, D., Wang, Y., Johansson, J., Zheng,  
521 J., Yang, Y., Shang, D., Wang, H., Liu, Q., Chan, C., Wang, T., Bannan, T. J., Priestley, M.,  
522 Percival, C. J., Shallcross, D. E., Lu, K., Guo, S., Hu, M., and Hallquist, M.: Chlorine  
523 oxidation of VOCs at a semi-rural site in Beijing: significant chlorine liberation from ClNO<sub>2</sub>  
524 and subsequent gas- and particle-phase Cl–VOC production, *Atmos Chem Phys*, 18, 13013–  
525 13030, <https://doi.org/10.5194/acp-18-13013-2018>, 2018.
- 526 Cai, X., Ziemba, L. D., and Griffin, R. J.: Secondary aerosol formation from the oxidation of  
527 toluene by chlorine atoms, *Atmos Environ*, 42, 7348–7359,  
528 <https://doi.org/10.1016/j.atmosenv.2008.07.014>, 2008.
- 529 Chang, C.-T., Liu, T.-H., and Jeng, F.-T.: Atmospheric concentrations of the Cl atom, ClO  
530 radical, and HO radical in the coastal marine boundary layer, *Environ. Res.*, 94, 67–74,  
531 <https://doi.org/10.1016/j.envres.2003.07.008>, 2004.
- 532 Chen, M., Yin, M., Su, Y., Li, R., Liu, K., Wu, Z., and Weng, X.: Atmospheric heterogeneous  
533 reaction of chlorobenzene on mineral  $\alpha$ -Fe<sub>2</sub>O<sub>3</sub> particulates: a chamber experiment study,  
534 *Front. Environ. Sci. Eng.*, 17, 134, <https://doi.org/10.1007/s11783-023-1734-9>, 2023.





- 535 Cubison, M. J. and Jimenez, J. L.: Statistical precision of the intensities retrieved from  
536 constrained fitting of overlapping peaks in high-resolution mass spectra, *Atmos. Meas. Tech.*,  
537 8, 2333–2345, <https://doi.org/10.5194/amt-8-2333-2015>, 2015.
- 538 DeMore, W. B., Sander, N. P., Golden, D. M., Hampson, R. F., Kurylo, M. J., Howard, C. J.,  
539 Ravishankara, A. R., Kolb, C. E., and Molina, M. J.: *Chemical Kinetics and Photochemical*  
540 *Data for Use in Stratospheric Modeling*, JPL Publication, 1997.
- 541 Ehn, M., Junninen, H., Petäjä, T., Kurtén, T., Kerminen, V.-M., Schobesberger, S., Manninen,  
542 H. E., Ortega, I. K., Vehkamäki, H., Kulmala, M., and Worsnop, D. R.: Composition and  
543 temporal behavior of ambient ions in the boreal forest, *Atmos. Chem. Phys.*, 10, 8513–8530,  
544 <https://doi.org/10.5194/acp-10-8513-2010>, 2010.
- 545 Ehn, M., Thornton, J. A., Kleist, E., Sipilä, M., Junninen, H., Pullinen, I., Springer, M.,  
546 Rubach, F., Tillmann, R., Lee, B., Lopez-Hilfiker, F., Andres, S., Acir, I.-H., Rissanen, M.,  
547 Jokinen, T., Schobesberger, S., Kangasluoma, J., Kontkanen, J., Nieminen, T., Kurtén, T.,  
548 Nielsen, L. B., Jørgensen, S., Kjaergaard, H. G., Canagaratna, M., Maso, M. D., Berndt, T.,  
549 Petäjä, T., Wahner, A., Kerminen, V.-M., Kulmala, M., Worsnop, D. R., Wildt, J., and  
550 Mentel, T. F.: A large source of low-volatility secondary organic aerosol, *Nature*, 506, 476–  
551 479, <https://doi.org/10.1038/nature13032>, 2014.
- 552 Eisele, F. L. and Tanner, D. J.: Measurement of the gas phase concentration of H<sub>2</sub>SO<sub>4</sub> and  
553 methane sulfonic acid and estimates of H<sub>2</sub>SO<sub>4</sub> production and loss in the atmosphere, *J*  
554 *Geophys Res Atmospheres*, 98, 9001–9010, <https://doi.org/10.1029/93jd00031>, 1993.
- 555 Europe, U. N. E. C. for: Globally Harmonized System of Classification and Labelling of  
556 Chemicals (GHS), *Glob. Harmon. Syst. Classif. Label. Chem. (GHS)*,  
557 <https://doi.org/10.18356/9789210019071>, 2023.
- 558 Finlayson-Pitts, B. J., Keoshian, C. J., Buehler, B., and Ezell, A. A.: Kinetics of reaction of  
559 chlorine atoms with some biogenic organics, *Int J Chem Kinet*, 31, 491–499,  
560 [https://doi.org/10.1002/\(sici\)1097-4601\(1999\)31:7<491::aid-kin4>3.0.co;2-e](https://doi.org/10.1002/(sici)1097-4601(1999)31:7<491::aid-kin4>3.0.co;2-e), 1999.
- 561 Heinritzi, M., Simon, M., Steiner, G., Wagner, A. C., Kürten, A., Hansel, A., and Curtius, J.:  
562 Characterization of the mass-dependent transmission efficiency of a CIMS, *Atmos Meas*  
563 *Tech*, 9, 1449–1460, <https://doi.org/10.5194/amt-9-1449-2016>, 2016.
- 564 Henschler, D.: Toxicity of Chlorinated Organic Compounds: Effects of the Introduction of  
565 Chlorine in Organic Molecules, *Angewandte Chemie Int Ed Engl*, 33, 1920–1935,  
566 <https://doi.org/10.1002/anie.199419201>, 1994.



- 567 Huang, M., Wang, Z., Hao, L., and Zhang, W.: DFT study on the abstraction and addition of  
568 Cl atom with toluene, *Comput. Theor. Chem.*, 996, 44–50,  
569 <https://doi.org/10.1016/j.comptc.2012.07.011>, 2012.
- 570 Huang, Y., Zhao, R., Charan, S. M., Kenseth, C. M., Zhang, X., and Seinfeld, J. H.: Unified  
571 Theory of Vapor–Wall Mass Transport in Teflon-Walled Environmental Chambers, *Environ.*  
572 *Sci. Technol.*, 52, 2134–2142, <https://doi.org/10.1021/acs.est.7b05575>, 2018.
- 573 Jahn, L. G., McPherson, K. N., and Ruiz, L. H.: Effects of Relative Humidity and Photoaging  
574 on the Formation, Composition, and Aging of Ethylbenzene SOA: Insights from Chamber  
575 Experiments on Chlorine Radical-Initiated Oxidation of Ethylbenzene, *ACS Earth Space*  
576 *Chem.*, 8, 675–688, <https://doi.org/10.1021/acsearthspacechem.3c00279>, 2024.
- 577 Keene, William. C., Khalil, M. A. K., Erickson, David. J., McCulloch, A., Graedel, T. E.,  
578 Lobert, J. M., Aucott, M. L., Gong, S. L., Harper, D. B., Kleiman, G., Midgley, P., Moore, R.  
579 M., Seuzaret, C., Sturges, W. T., Benkovitz, C. M., Koropalov, V., Barrie, L. A., and Li, Y.  
580 F.: Composite global emissions of reactive chlorine from anthropogenic and natural sources:  
581 Reactive Chlorine Emissions Inventory, *J. Geophys. Res.: Atmos.*, 104, 8429–8440,  
582 <https://doi.org/10.1029/1998jd100084>, 1999.
- 583 Knipping, E. M., Lakin, M. J., Foster, K. L., Jungwirth, P., Tobias, D. J., Gerber, R. B.,  
584 Dabdub, D., and Finlayson-Pitts, B. J.: Experiments and Simulations of Ion-Enhanced  
585 Interfacial Chemistry on Aqueous NaCl Aerosols, *Science*, 288, 301–306,  
586 <https://doi.org/10.1126/science.288.5464.301>, 2000.
- 587 Krechmer, J., Lopez-Hilfiker, F., Koss, A., Hutterli, M., Stoermer, C., Deming, B., Kimmel,  
588 J., Warneke, C., Holzinger, R., Jayne, J., Worsnop, D., Fuhrer, K., Gonin, M., and Gouw, J.  
589 de: Evaluation of a New Reagent-Ion Source and Focusing Ion–Molecule Reactor for Use in  
590 Proton-Transfer-Reaction Mass Spectrometry, *Anal Chem*, 90, 12011–12018,  
591 <https://doi.org/10.1021/acs.analchem.8b02641>, 2018.
- 592 Kulmala, M., Kontkanen, J., Junninen, H., Lehtipalo, K., Manninen, H. E., Nieminen, T.,  
593 Petäjä, T., Sipilä, M., Schobesberger, S., Rantala, P., Franchin, A., Jokinen, T., Järvinen, E.,  
594 Äijälä, M., Kangasluoma, J., Hakala, J., Aalto, P. P., Paasonen, P., Mikkilä, J., Vanhanen, J.,  
595 Aalto, J., Hakola, H., Makkonen, U., Ruuskanen, T., Mauldin, R. L., Duplissy, J., Vehkamäki,  
596 H., Bäck, J., Kortelainen, A., Riipinen, I., Kurtén, T., Johnston, M. V., Smith, J. N., Ehn, M.,  
597 Mentel, T. F., Lehtinen, K. E. J., Laaksonen, A., Kerminen, V.-M., and Worsnop, D. R.:  
598 Direct Observations of Atmospheric Aerosol Nucleation, *Science*, 339, 943–946,  
599 <https://doi.org/10.1126/science.1227385>, 2013.
- 600 Kürten, A., Rondo, L., Ehrhart, S., and Curtius, J.: Performance of a corona ion source for  
601 measurement of sulfuric acid by chemical ionization mass spectrometry, *Atmos Meas Tech*,  
602 4, 437–443, <https://doi.org/10.5194/amt-4-437-2011>, 2011.



- 603 Kürten, A., Rondo, L., Ehrhart, S., and Curtius, J.: Calibration of a Chemical Ionization Mass  
 604 Spectrometer for the Measurement of Gaseous Sulfuric Acid, *J Phys Chem*, 116, 6375–6386,  
 605 <https://doi.org/10.1021/jp212123n>, 2012.
- 606 Kürten, A., Bergen, A., Heinritzi, M., Leiminger, M., Lorenz, V., Piel, F., Simon, M., Sitals,  
 607 R., Wagner, A. C., and Curtius, J.: Observation of new particle formation and measurement of  
 608 sulfuric acid, ammonia, amines and highly oxidized organic molecules at a rural site in central  
 609 Germany, *Atmos Chem Phys*, 16, 12793–12813, <https://doi.org/10.5194/acp-16-12793-2016>,  
 610 2016.
- 611 Liu, X., Qu, H., Huey, L. G., Wang, Y., Sjostedt, S., Zeng, L., Lu, K., Wu, Y., Hu, M., Shao,  
 612 M., Zhu, T., and Zhang, Y.: High Levels of Daytime Molecular Chlorine and Nitryl Chloride  
 613 at a Rural Site on the North China Plain, *Environ Sci Technol*, 51, 9588–9595,  
 614 <https://doi.org/10.1021/acs.est.7b03039>, 2017.
- 615 Lu, Y., Liu, L., Ning, A., Yang, G., Liu, Y., Kurtén, T., Vehkamäki, H., Zhang, X., and  
 616 Wang, L.: Atmospheric Sulfuric Acid-Dimethylamine Nucleation Enhanced by  
 617 Trifluoroacetic Acid, *Geophys Res Lett*, 47, <https://doi.org/10.1029/2019gl085627>, 2020.
- 618 Ma, W., Chen, X., Xia, M., Liu, Y., Wang, Y., Zhang, Y., Zheng, F., Zhan, J., Hua, C., Wang,  
 619 Z., Wang, W., Fu, P., Kulmala, M., and Liu, Y.: Reactive Chlorine Species Advancing the  
 620 Atmospheric Oxidation Capacities of Inland Urban Environments, *Environ. Sci. Technol.*, 57,  
 621 14638–14647, <https://doi.org/10.1021/acs.est.3c05169>, 2023.
- 622 Molteni, U., Bianchi, F., Klein, F., Haddad, I. E., Frege, C., Rossi, M. J., Dommen, J., and  
 623 Baltensperger, U.: Formation of highly oxygenated organic molecules from aromatic  
 624 compounds, *Atmos Chem Phys*, 18, 1909–1921, <https://doi.org/10.5194/acp-18-1909-2018>,  
 625 2018.
- 626 Orlando, J. J., Tyndall, G. S., Apel, E. C., Riemer, D. D., and Paulson, S. E.: Rate coefficients  
 627 and mechanisms of the reaction of Cl-atoms with a series of unsaturated hydrocarbons under  
 628 atmospheric conditions, *Int. J. Chem. Kinet.*, 35, 334–353, <https://doi.org/10.1002/kin.10135>,  
 629 2003.
- 630 Peng, X., Wang, W., Xia, M., Chen, H., Ravishankara, A. R., Li, Q., Saiz-Lopez, A., Liu, P.,  
 631 Zhang, F., Zhang, C., Xue, L., Wang, X., George, C., Wang, J., Mu, Y., Chen, J., and Wang,  
 632 T.: An unexpected large continental source of reactive bromine and chlorine with significant  
 633 impact on wintertime air quality, *Natl. Sci. Rev.*, 8, nwaa304,  
 634 <https://doi.org/10.1093/nsr/nwaa304>, 2020.
- 635 Peng, X., Wang, T., Wang, W., Ravishankara, A. R., George, C., Xia, M., Cai, M., Li, Q.,  
 636 Salvador, C. M., Lau, C., Lyu, X., Poon, C. N., Mellouki, A., Mu, Y., Hallquist, M., Saiz-  
 637 Lopez, A., Guo, H., Herrmann, H., Yu, C., Dai, J., Wang, Y., Wang, X., Yu, A., Leung, K.,



- 638 Lee, S., and Chen, J.: Photodissociation of particulate nitrate as a source of daytime  
639 tropospheric Cl<sub>2</sub>, *Nat Commun*, 13, 939, <https://doi.org/10.1038/s41467-022-28383-9>, 2022.
- 640 Priestley, M., Breton, M. le, Bannan, T. J., Worrall, S. D., Bacak, A., Smedley, A. R. D.,  
641 Reyes-Villegas, E., Mehra, A., Allan, J., Webb, A. R., Shallcross, D. E., Coe, H., and  
642 Percival, C. J.: Observations of organic and inorganic chlorinated compounds and their  
643 contribution to chlorine radical concentrations in an urban environment in northern Europe  
644 during the wintertime, *Atmos Chem Phys*, 18, 13481–13493, [https://doi.org/10.5194/acp-18-](https://doi.org/10.5194/acp-18-13481-2018)  
645 [13481-2018](https://doi.org/10.5194/acp-18-13481-2018), 2018.
- 646 Ragains, M. L. and Finlayson-Pitts, B. J.: Kinetics and Mechanism of the Reaction of Cl  
647 Atoms with 2-Methyl-1,3-butadiene (Isoprene) at 298 K, *J. Phys. Chem. A*, 101, 1509–1517,  
648 <https://doi.org/10.1021/jp962786m>, 1997.
- 649 Riva, M., Healy, R. M., Flaud, P.-M., Perraudin, E., Wenger, J. C., and Villenave, E.: Gas-  
650 and Particle-Phase Products from the Chlorine-Initiated Oxidation of Polycyclic Aromatic  
651 Hydrocarbons., *J Phys Chem*, 119, 11170–81, <https://doi.org/10.1021/acs.jpca.5b04610>,  
652 2015.
- 653 Shang, D., Peng, J., Guo, S., Wu, Z., and Hu, M.: Secondary aerosol formation in winter haze  
654 over the Beijing-Tianjin-Hebei Region, China, *Front. Environ. Sci. Eng.*, 15, 34,  
655 <https://doi.org/10.1007/s11783-020-1326-x>, 2021.
- 656 Shi, J. and Bernhard, M. J.: Kinetic studies of Cl-atom reactions with selected aromatic  
657 compounds using the photochemical reactor-FTIR spectroscopy technique, *Int. J. Chem.*  
658 *Kinet.*, 29, 349–358, [https://doi.org/10.1002/\(sici\)1097-4601\(1997\)29:5<349::aid-](https://doi.org/10.1002/(sici)1097-4601(1997)29:5<349::aid-kin5>3.0.co;2-u)  
659 [kin5>3.0.co;2-u](https://doi.org/10.1002/(sici)1097-4601(1997)29:5<349::aid-kin5>3.0.co;2-u), 1997.
- 660 Sokolov, O., Hurley, M. D., Wallington, T. J., Kaiser, E. W., Platz, J., Nielsen, O. J., Berho,  
661 F., Rayez, M.-T., and Lesclaux, R.: Kinetics and Mechanism of the Gas-Phase Reaction of Cl  
662 Atoms with Benzene, *J. Phys. Chem. A*, 102, 10671–10681,  
663 <https://doi.org/10.1021/jp9828080>, 1998.
- 664 Tham, Y. J., Wang, Z., Li, Q., Yun, H., Wang, W., Wang, X., Xue, L., Lu, K., Ma, N., Bohn,  
665 B., Li, X., Kecorius, S., Größ, J., Shao, M., Wiedensohler, A., Zhang, Y., and Wang, T.:  
666 Significant concentrations of nitryl chloride sustained in the morning: investigations of the  
667 causes and impacts on ozone production in a polluted region of northern China, *Atmos Chem*  
668 *Phys*, 16, 14959–14977, <https://doi.org/10.5194/acp-16-14959-2016>, 2016.
- 669 Thornton, J. A., Kercher, J. P., Riedel, T. P., Wagner, N. L., Cozic, J., Holloway, J. S., Dubé,  
670 W. P., Wolfe, G. M., Quinn, P. K., Middlebrook, A. M., Alexander, B., and Brown, S. S.: A  
671 large atomic chlorine source inferred from mid-continental reactive nitrogen chemistry,  
672 *Nature*, 464, 271–274, <https://doi.org/10.1038/nature08905>, 2010.



- 673 Wang, C., Collins, D. B., and Abbatt, J. P. D.: Indoor Illumination of Terpenes and Bleach  
 674 Emissions Leads to Particle Formation and Growth, *Environ. Sci. Technol.*, 53, 11792–  
 675 11800, <https://doi.org/10.1021/acs.est.9b04261>, 2019.
- 676 Wang, C., Liggio, J., Wentzell, J. J. B., Jorga, S., Folkerson, A., and Abbatt, J. P. D.:  
 677 Chloramines as an important photochemical source of chlorine atoms in the urban  
 678 atmosphere, *Proc. Natl. Acad. Sci.*, 120, e2220889120,  
 679 <https://doi.org/10.1073/pnas.2220889120>, 2023.
- 680 Wang, D. S. and Ruiz, L. H.: Secondary organic aerosol from chlorine-initiated oxidation of  
 681 isoprene, *Atmos Chem Phys*, 17, 13491–13508, <https://doi.org/10.5194/acp-17-13491-2017>,  
 682 2017.
- 683 Wang, D. S., Masoud, C. G., Modi, M., and Ruiz, L. H.: Isoprene-Chlorine Oxidation in the  
 684 Presence of NO<sub>x</sub> and Implications for Urban Atmospheric Chemistry., *Environ Sci Technol*,  
 685 <https://doi.org/10.1021/acs.est.1c07048>, 2022.
- 686 Wang, L., Arey, J., and Atkinson, R.: Reactions of Chlorine Atoms with a Series of Aromatic  
 687 Hydrocarbons, *Environ Sci Technol*, 39, 5302–5310, <https://doi.org/10.1021/es0479437>,  
 688 2005.
- 689 Wang, S., Wu, R., Berndt, T., Ehn, M., and Wang, L.: Formation of Highly Oxidized Radicals  
 690 and Multifunctional Products from the Atmospheric Oxidation of Alkylbenzenes, *Environ.*  
 691 *Sci. Technol.*, 51, 8442–8449, <https://doi.org/10.1021/acs.est.7b02374>, 2017.
- 692 Wang, Y., Riva, M., Xie, H., Heikkinen, L., Schallhart, S., Zha, Q., Yan, C., He, X.-C.,  
 693 Peräkylä, O., and Ehn, M.: Formation of highly oxygenated organic molecules from chlorine-  
 694 atom-initiated oxidation of alpha-pinene, *Atmos Chem Phys*, 20, 5145–5155,  
 695 <https://doi.org/10.5194/acp-20-5145-2020>, 2020.
- 696 Wang, Y., Li, C., Zhang, Y., Li, Y., Yang, G., Yang, X., Wu, Y., Yao, L., Zhang, H., and  
 697 Wang, L.: Secondary reactions of aromatics-derived oxygenated organic molecules lead to  
 698 plentiful highly oxygenated organic molecules within an intraday OH exposure, *Atmos.*  
 699 *Chem. Phys.*, 24, 7961–7981, <https://doi.org/10.5194/acp-24-7961-2024>, 2024.
- 700 Wingenter, O. W., Sive, B. C., Blake, N. J., Blake, D. R., and Rowland, F. S.: Atomic  
 701 chlorine concentrations derived from ethane and hydroxyl measurements over the equatorial  
 702 Pacific Ocean: Implication for dimethyl sulfide and bromine monoxide, *J. Geophys. Res.*:  
 703 *Atmos.*, 110, <https://doi.org/10.1029/2005jd005875>, 2005.
- 704 Wu, Y., Huo, J., Yang, G., Wang, Y., Wang, L., Wu, S., Yao, L., Fu, Q., and Wang, L.:  
 705 Measurement report: Production and loss of atmospheric formaldehyde at a suburban site of



- 706 Shanghai in summertime, *Atmos. Chem. Phys.*, 23, 2997–3014, [https://doi.org/10.5194/acp-](https://doi.org/10.5194/acp-23-2997-2023)  
707 [23-2997-2023](https://doi.org/10.5194/acp-23-2997-2023), 2023.
- 708 Xu, L., Møller, K. H., Crounse, J. D., Kjaergaard, H. G., and Wennberg, P. O.: New Insights  
709 into the Radical Chemistry and Product Distribution in the OH-Initiated Oxidation of  
710 Benzene, *Environ. Sci. Technol.*, 54, 13467–13477, <https://doi.org/10.1021/acs.est.0c04780>,  
711 2020.
- 712 Yang, G., Huo, J., Wang, L., Wang, Y., Wu, S., Yao, L., Fu, Q., and Wang, L.: Total OH  
713 Reactivity Measurements in a Suburban Site of Shanghai, *J Geophys Res Atmospheres*, 127,  
714 <https://doi.org/10.1029/2021jd035981>, 2022.
- 715 Yang, X., Ren, S., Wang, Y., Yang, G., Li, Y., Li, C., Wang, L., Yao, L., and Wang, L.:  
716 Volatility Parametrization of Low-Volatile Components of Ambient Organic Aerosols Based  
717 on Molecular Formulas, *Environ. Sci. Technol.*, <https://doi.org/10.1021/acs.est.3c02073>,  
718 2023.
- 719 Zhao, Y., Thornton, J. A., and Pye, H. O. T.: Quantitative constraints on autoxidation and  
720 dimer formation from direct probing of monoterpene-derived peroxy radical chemistry, *Proc*  
721 *National Acad Sci*, 115, 12142–12147, <https://doi.org/10.1073/pnas.1812147115>, 2018.
- 722